RSC Advances

PAPER

View Article Online
View Journal | View Issue

Cite this: *RSC Adv.*, 2019, **9**, 33302

Dual-mode US/MRI nanoparticles delivering siRNA and Pt(IV) for ovarian cancer treatment†

Yanhua Zhang,‡[a] Hui Huang,‡[a] Hao Fu,[a] Meng Zhao,[a] Zhihua Wu,[a] Yang Dong,[a] He Li,[b] Yourong Duan [a] and Ying Sun*[a]

Received 16th May 2019
Accepted 6th October 2019

DOI: 10.1039/c9ra03681d

rsc.li/rsc-advances

As known to all, ovarian cancer ranks the most lethal of the gynecological malignancies. The antitumor drugs based on platinum are first-line chemotherapy drugs for ovarian cancer. However, their therapeutic efficiency is severely limited owing to dose-limiting toxicities of platinum. New theranostic strategies to overcome chemotherapy toxicity is highly desirable. Meanwhile, the real-time treating effect is not visible for doctors. Herein, we constructed PFH/siRNA/Fe_3O_4@Pt(IV) NPs-cRGD (NPs-cRGD) for precise theranostics against ovarian tumors with real-time imaging. The NPs-cRGD had a good storage stability and resisted the serum-induced aggregation, which was beneficial for drug delivery. Additionally, gel-retardation assay demonstrated that the NPs-cRGD exhibited great protection to siRNA to resist nuclease degradation. *In vitro*, the NPs-cRGD showed good dual-mode US/MRI imaging and the relative imaging research was also discussed. Moreover, the *in vitro* experiments indicated that the NPs-cRGD with US exhibited excellent antitumor therapeutic efficiency, resulting from the cRGD ligands and US exposure enhanced the cellular uptake efficiency. Thus, the dual-mode nanoparticles in this work may provide precious insight into the development of various multi-mode nanoplatforms delivering drugs or genes for precise theranostics against various cancer.

Introduction

The mortality rate of ovarian cancer is number one in female malignant tumors of the genital system according to Siegel, *et al.*[1] In clinics, the basic drug of chemotherapy for ovarian cancer is platinum, for example neutral, square planar coordination complex, cisplatin [CDDP, *cis*-diamminedichloroplatinum(II)],[2] but unfortunately, the side effects of cisplatin, which was recognized as the most active single agent for treating advanced ovarian cancer, are bad resulting in problems in the kidney, nerves, blood *etc.*[3–5] So we attempt to find some better way to treat ovarian cancer so as to enhance the therapy efficiency.

At present, more and more efforts have been made to treat ovarian cancer, including some new medicine and methods.[6] Fortunately, the platinum(IV) (Pt(IV)) prodrug as the derivative of platinum(II) (Pt(II)) which has more anticancer activity[7,8] and less toxicity[9,10] shows an exciting result. Meanwhile, in the past decade, the research to small interfering RNAs (siRNAs) as an emerging therapy and one kind of drugs to treat diseases especially neoplasms has become more and more deep and meaningful.[11,12] Considering the survivin protein may be against the death of cells,[13–15] we try to combine Pt(IV) with siRNA of survivin to enhance antitumor effect. Furthermore, in recent years, due to the unique physical and chemical properties of the nanoparticles, such as: good controllability, going through the biological barrier, improving the target property through the enhanced permeability and retention (EPR) effect, the nanoparticles has opened an new field of treating diseases especially tumors.[16]

Besides, it's invisible and inconvenient for physicians to monitor disease situation while treating tumors, so we gave birth to combing therapy with ultrasound imaging and magnetic resonance imaging (MRI). Perfluorohexane (PFH) is one of the phase-shifted ultrasound contrast agents, whose boiling point (56 °C) is higher than that of traditional perfluoropentane (PFP, 29 °C),[17] so it has the advantage of steady existing in bodies. In previous work,[6] a multifunctional nanoplatform based on phase-transitional nanoparticles with ultrasound (US) exhibited excellent echogenic signals and brilliant therapeutic efficacy has been constructed. But some problems, including the low phase-transition efficiency and poor resolution, puzzled us. Owing to the Fe_3O_4 nanoparticles probably improving the phase shifting efficiency of PFH,[18,19] we intend to encapsulate the Fe_3O_4 nanoparticles into nanoparticles to enhance the ultrasound imaging of nanoparticles.

[a]*State Key Laboratory of Oncogenes and Related Genes, Shanghai Cancer Institute, Renji Hospital, School of Medicine, Shanghai Jiao Tong University, Shanghai 200032, China. E-mail: ysun@shsci.org*

[b]*Traditional Chinese Medicine Department, Renji Hospital, School of Medicine, Shanghai Jiao Tong University, Shanghai 200127, China*

† Electronic supplementary information (ESI) available. See DOI: 10.1039/c9ra03681d

‡ The two authors have contributed equally to this work.

Furthermore, the Fe_3O_4 nanoparticles could be also used as a negative contrast agent in MRI image[20,21] to improve the deep tissue images. Comparing to safe, convenient, inexpensive ultrasound imaging, the MRI shows a better and clearer images of deep tissues. Therefore, it's expected and exciting to synthesize a nanoplatform with dual-mode US/MRI imaging to monitor disease progression.

In this study, we designed a nanoplatform siRNA/Fe_3O_4@Pt(IV) NPs-cRGD (NPs-cRGD) (in Fig. 1) encapsulating Pt(IV), siRNA, PFH and Fe_3O_4 nanoparticles for dual-mode US/MRI imaging. And some methods and technologies, such as: measuring size and zeta potential, transmission electron microscopy and X-ray polycrystalline, were used to characterize the NPs-cRGD. Then we explored the storage stability of the NPs-cRGD and the protection of the NPs-cRGD to siRNA. Besides, the ultrasound imaging and MRI of the NPs-cRGD were measured. Finally, the toxicity and uptake of the NPs-cRGD were detected.

Results and discussion

Connection of DEAPA to Fe_3O_4 nanoparticles

Before connecting DEAPA (one organic matter containing amino) to carboxyl on the surface of the Fe_3O_4 nanoparticles, the quantity of carboxyl was 1.322 mmol mL^{-1} and the zeta potential of the Fe_3O_4 nanoparticles was -31.1 ± 2.82 mV (Fig. S1C†). And after reacting with DEAPA, carboxyl on the surface of the Fe_3O_4 nanoparticles was 0.214 mmol mL^{-1} and the zeta potential of the Fe_3O_4 nanoparticles was $+4.82 \pm 0.85$ mV (Fig. S1D†). The above results confirmed the successful connection of DEAPA to the Fe_3O_4 nanoparticles, so siRNA with negative charges could be absorbed onto the surface of the Fe_3O_4 nanoparticles. Before and after reacting with the DEAPA, the size of the Fe_3O_4 nanoparticles was about 30 nm, and polymer dispersity index (PDI) was 0.29 (Fig. S1A and B†). As shown in Fig. 2D, there existed no remanence and coercivity in the Fe_3O_4 nanoparticles, the saturation magnetization of which was 15.5 emu g^{-1}. This result demonstrated that, superparamagnetic characteristics was preserved at room temperature after connecting DEAPA.

Characterization of NPs-cRGD

The size of NPs-cRGD was 307.9 ± 19.80 nm, and PDI was 0.273 ± 0.02 (Fig. 2A). The zeta potential analysis showed that the surface charge of the NPs-cRGD was $+10.9 \pm 0.31$ mV in aqueous solution (Fig. S2†). As shown in Fig. 2B, the TEM

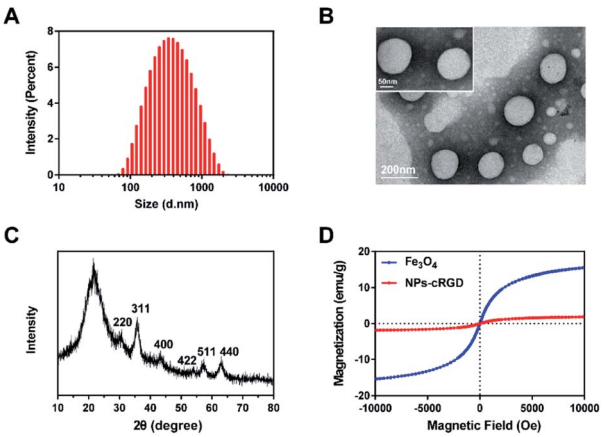

Fig. 2 Characterization of NPs-cRGD. (A) Size distribution of NPs-cRGD. (B) TEM image of NPs-cRGD. (C) XRD pattern of NPs-cRGD. (D) Magnetization *versus* field of NPs-cRGD and Fe_3O_4 nanoparticles at room temperature.

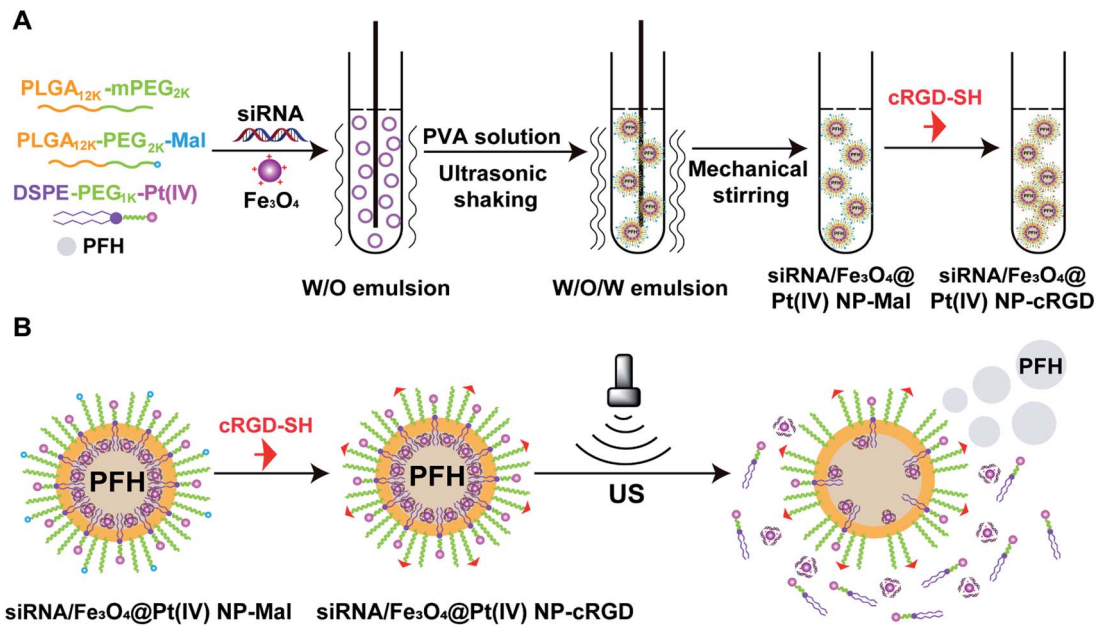

Fig. 1 Synthesis of siRNA/Fe_3O_4@Pt(IV) NPs-cRGD (NPs-cRGD). (A) Synthetic route used to prepare NPs-cRGD. (B) The schematic illustration of the phase transition of NPs-cRGD.

images revealed regular morphologies of the NPs-cRGD. In addition, the structure of the Fe_3O_4 nanoparticles in NPs-cRGD was analyzed by XRD in Fig. 2C. The results showed that the X-ray diffraction (XRD) curve character of NPs-cRGD was almost similar to that of Fe_3O_4 nanoparticles, and the peaks had the diffraction of (220), (311), (400), (422), (510), (440) at 30.1, 35.5, 43.1, 53.5, 57.0, and 62.6°, respectively, suggesting the existence of Fe_3O_4 nanoparticles.[22] Then, we explored the magnetic character of the NPs-cRGD (Fig. 2D). Due to the nonmagnetic materials, the saturation magnetization of the NPs-cRGD is 1.9 emu g^{-1}, which was smaller than that of the Fe_3O_4 nanoparticles. Both NPs-cRGD and Fe_3O_4 nanoparticles had no remanence and coercivity, demonstrating that they had the superparamagnetic characteristics at room temperature. At last, the encapsulation rate of siRNA measured by a fluorescence spectrometer was 94.28%. The drug loading efficiencies (DL%) of the NPs-cRGD was 3.46 ± 0.33%. Therefore, the NPs-cRGD was synthesized successfully and possessed good properties which was very beneficial for further applications.

Stability of NPs-cRGD

Staying at 4 °C for 14 days, the average size was about 300 nm and the zeta potential was about +10 mV (Fig. 3A). Meanwhile, the value of PDI didn't change significantly within 14 days at 4 °C (Fig. S3†). The above results suggested that the NPs-cRGD had a good storage stability. Moreover, the serum stability of NPs-cRGD were evaluated by a serum-induced aggregation assay (Fig. 3B). The turbidity of the free siRNA group gradually increased with time, and the turbidity value was 1.95 ± 0.04 at 14 d. However, the turbidity of NPs-cRGD kept stably for 14 days, indicating that NPs-cRGD resisted the serum-induced aggregation and remained stable in the blood circulation.

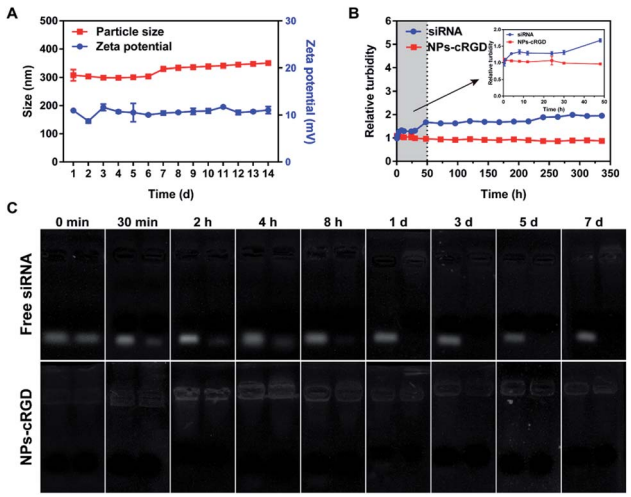

Fig. 3 The stability of NPs-cRGD. (A) Storage stability of NPs-cRGD at 4 °C. (B) Serum stability of NPs-cRGD. Serum-induced aggregation assay was monitored based on turbidity at the indicated time. (C) The potential of NPs-cRGD to resist nuclease degradation. NPs-cRGD was incubated without nuclease (left) or with nuclease (right) for different time. The data are presented as the mean ± SD of three independent experiments.

As shown in Fig. 3C, siRNA encapsulated in NPs-cRGD was retained at the beginning site and the free siRNA moved out. So we thought the siRNA was successfully encapsulated into NPs-cRGD and the reason might be that siRNA could be tightly attracted to the Fe_3O_4 nanoparticles and DOTAP with positive charges. And after 5 days, the siRNA encapsulated in the NPs-cRGD still didn't move out, which indicated the encapsulated siRNA could steady stay in NPs-cRGD for nearly one week at 4 °C. Besides, free siRNA incubating with the ribonuclease (RNase) was degraded within one day, but the siRNA encapsulated in NPs-cRGD incubating with RNase was still stable for five days. Therefore, the NPs-cRGD showed the great protection to siRNA to resist nuclease degradation.

MRI of NPs-cRGD *in vitro*

Varying the concentration of iron from 2.5 to 320 μg mL^{-1}, the higher the concentration of Fe_3O_4 nanoparticles was, the stronger the T_2-weighted MRI was (Fig. 4A). The corresponding concentration of Fe_3O_4 nanoparticles encapsulated in the NPs-cRGD was represented by the blue curve (Fig. 4B). The MRI signal intensity of different groups was shown as the red curve (Fig. 4B). The T_2 relaxation time of the NPs-cRGD was tested by MesoMR. The linear fit was obtained between the iron concentration and the T_2 relaxation rates ($1/T_2$) with $R^2 = 58.64$ mM^{-1} s^{-1} similar to that of others[22] (Fig. 4C). The MRI signal intensity decreased with the increasing iron concentration, which indicated that the NPs-cRGD produced the magnetic resonance contrast on a transverse photon relaxation-time-weighted sequence.

Ultrasound imaging of NPs-cRGD *in vitro*

As shown in Fig. 5A(a–g), as the concentration of Fe_3O_4 nanoparticles increased from 0 μg mL^{-1} to 320 μg mL^{-1}, the ultrasound imaging was gradually enhanced and reached the strongest imaging at 320 μg mL^{-1}. Then, as depicted in

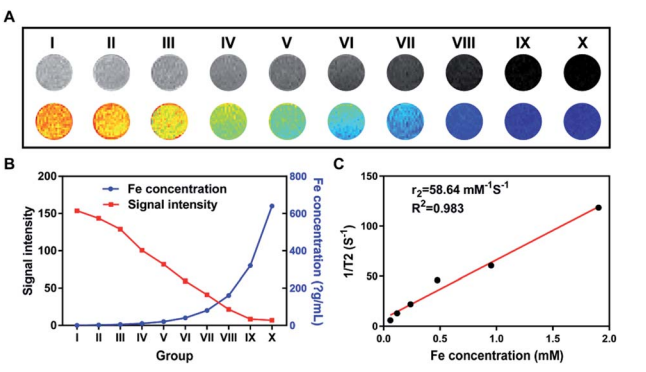

Fig. 4 The MRI of nanoparticles *in vitro*. (A) *In vitro* T_2-weighted MR image of NPs-cRGD. (I) Deionized water; (II) siRNA@Pt(IV) NPs-cRGD; (III–X) NPs-cRGD with iron concentration 2.5, 5, 10, 20, 40, 80, 160, 320 μg mL^{-1}, respectively. (B) Different iron concentrations (blue curve) and MR signal intensities of NPs-cRGD (red curve) in groups (I–X). (C) T_2 relaxation rates ($1/T_2$ (s^{-1})) of NPs-cRGD at different iron concentrations. The data are presented as the mean ± SD of three independent experiments.

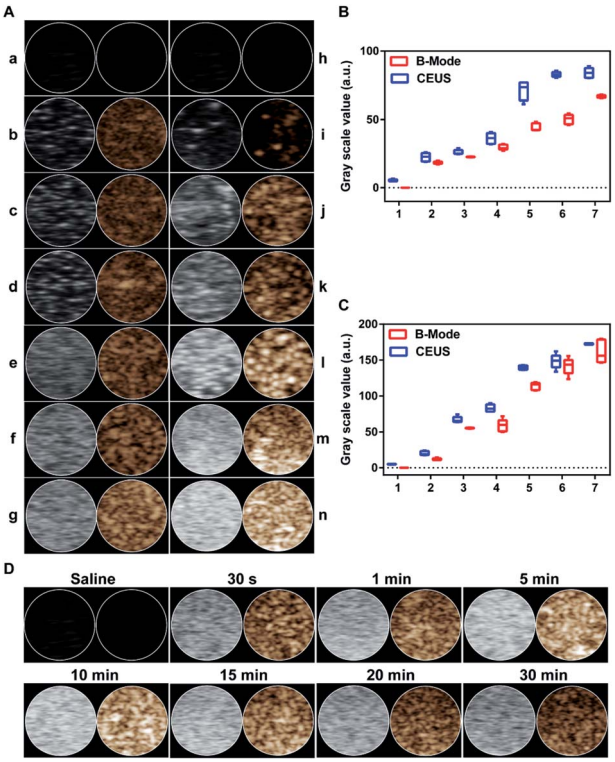

Fig. 5 US imaging *in vitro*. (A) (a–g) US imaging of saline (a) and different concentrations of iron in NPs-cRGD ((b–g) separately represent 0, 10, 40, 80, 160, 320 μg mL^{-1}). (h–n) US imaging of saline (h) and different concentrations of NPs-cRGD ((i–n) separately represent 0.25, 0.5, 1.0, 2.0, 4.0, 8.0 mg mL^{-1}). B-Mode (left) and contrast-enhanced ultrasound (CEUS) (right) image of NPs-cRGD. (B and C) Corresponding quantification of gray scale values of NPs-cRGD changed along with the changes in concentrations of iron (B) and nanoparticles (C). The data are shown as the mean ± SD of three independent experiments iron. (D) US imaging of saline and 8 mg mL^{-1} NPs-cRGD after different US exposure times. B-Mode (left) and CEUS (right).

Fig. 5A(h–n), on the condition of 320 μg mL^{-1} Fe_3O_4 nanoparticles, the ultrasound imaging of the NPs-cRGD got increasingly weak with the variation of concentration of nanoparticles' materials from 8 mg mL^{-1} to 0.25 mg mL^{-1}. Fig. 5B and C demonstrated that the acoustic signal intensity value changed at different concentrations of Fe_3O_4 nanoparticles and nanoparticles' materials. According to Fig. 5D and S3,† the ultrasound images of the NPs-cRGD clearly exhibited increasingly enriched echo signal and contrast enhancement within 10 min. However, the ultrasound signals gradually decreased over the next 20 min. Additionally, the duration of ultrasound imaging of the NPs-cRGD was longer than that of nanoparticles without Fe_3O_4 nanoparticles,[16] probably resulting from that Fe_3O_4 nanoparticles acted as nucleation agents to promote phase transition thus to improve conversion efficiency.[23]

Antitumor effects of NPs-cRGD under US exposure *in vitro*

To measure the cellular uptake of nanoparticles, SKOV3 cells was stained with Prussian blue stain, which reacts with iron presenting in the magnetite core yielding a characteristic blue color. In Fig. 6, compared with other nanoparticles groups, cells treated with NPs-cRGD + US contained more iron at the same concentration for 24 h. Additionally, as the concentration of nanoparticles increased, the amount of intracellular iron increased. The above results demonstrated that the cRGD ligands and ultrasound exposure enhanced the cellular uptake efficiency.

In Fig. 7A, the viability of cells did not exhibit a significant change at 24 h, 48 h and 72 h, even at the concentrations of nanoparticles materials up to 1000 μg mL^{-1}, which indicated that the materials of NPs-cRGD had relatively low cytotoxicity and can be a good drug nano-carrier. The same results of the normal cell were shown in Fig. S5A.† In addition, to determine the antitumor effects of NPs-cRGD under US exposure, the MTT assay was used for measuring the cytotoxicity of different concentrations of nanoparticles at different times.

According to Fig. 7B–D, the antitumor effect of nanoparticles exhibited apparent concentration-dependent and time-dependent feature. As shown in Fig. 7C, the half maximal inhibitory concentration (IC_{50}) were 26 μM, 18 μM, 14 μM and 13 μM, respectively, when the cells were incubated with free Pt, NPs, NPs-cRGD and NPs-cRGD + US for 48 h. The antitumor efficiency of the NPs-cRGD was higher than that of the NPs because the introduction of the cRGD ligands improved cellular uptake by ligand–receptor recognition.[24–26] In addition, compared to the equivalent dose of NPs-cRGD, the cytotoxicity of NPs-cRGD with US increased obviously, whose cell viability value was measured as 37.23 ± 5.87% at the concentration of 24 μM, resulting from that ultrasound promoted drug release and accelerated intracellular uptake to enhance cytotoxicity. So it is possible for us to reach the same therapeutic effect by using less dose of platinum and we believe that it will be hopeful to reduce the system toxicity. And surprisingly, compared to the SKOV3 cells, the IC_{50} of L929 cell were 47 μM, 130 μM, 103 μM and 132 μM, respectively, when the normal cells were incubated with free Pt, NPs, NPs-cRGD and NPs-cRGD + US for 48 h (Fig. S5B–D†). It's easy to find that the NPs and NPs-cRGD had more serious cell toxicity than Pt to SKOV3 cells and had less killing cell ability than Pt to normal cells. That is to say, the NPs and NPs-cRGD owned the better therapeutic effects and less adverse effects than Pt. We guessed the reason might be the absence of integrin receptors on normal cells.

Experimental section

Materials

Poly(lactic-*co*-glycolic acid)–COOH (PLGA–COOH) (lactide : glycolide = 75 : 25, M_w = 12 500) was purchased from Jinan

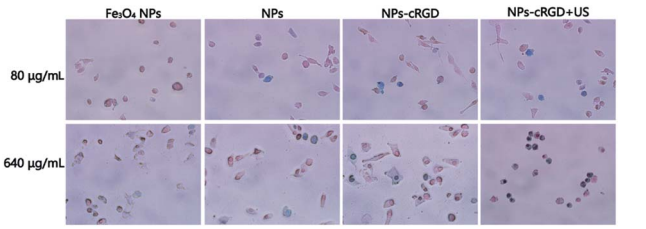

Fig. 6 Photomicrographs show Prussian blue staining of SKOV3 cells.

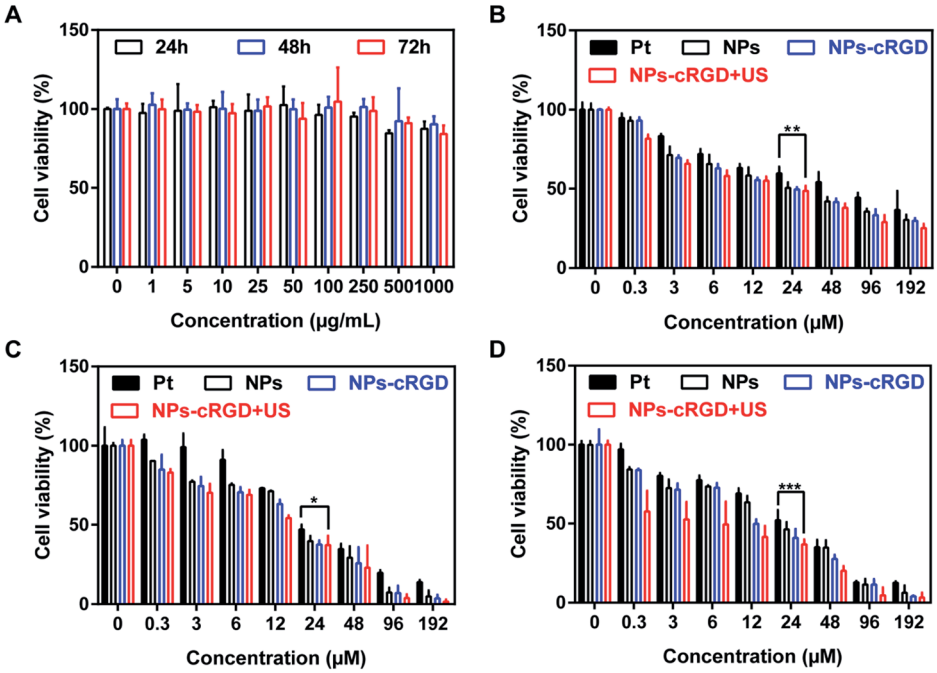

Fig. 7 (A) Cell viability of SKOV3 cells with the treatment of various concentrations of Fe_3O_4@ NPs-cRGD for 24 h, 48 h and 72 h. (B–D) Cell viability of the SKOV3 cells treated with various concentrations of Pt(II), siRNA/Fe_3O_4@Pt(IV) NPs, NPs-cRGD and NPs-cRGD + US for 24 h (B), 48 h (C) and 72 h (D). The data are presented as the mean ± SD of three independent experiments.

Daigang Biomaterial Co., Ltd. Poly(vinyl alcohol) (PVA, 88% M_w = 22 000) was purchased from Acros Organics Company (Geel, Belgium). *N*-Hydroxysuccinimide (NHS, M_w = 115) was obtained from Sigma Aldrich Company and *N*-(3-dimethylaminopropyl)-*N*′-ethylcarbodiimide hydrochloride (EDC·HCl) was purchased from GL Biochem (Shanghai) Ltd. Methoxypolyethylene glycol amino group ($mPEG_{2000}$–NH_2, M_w = 2000), poly(L-lactide-*co*-glycolide)$_{12\,000}$–polyethylene glycol$_{2000}$–maleimide ($PLGA_{12\,500}$–PEG_{2000}–Mal) and 2-distearoyl-*sn*-glycero-3-phosphoethanolamine–polyethylene glycol$_{1000}$–NH_2 (DSPE–PEG_{1000}–NH_2) were purchased from Shanghai Pengshuo Biotechnology Co., Ltd. Fe_3O_4 nanoparticles (Fe_3O_4 NPs) were from Henan Huier Nano Technology Co., Ltd. (Henan, China). Cisplatin (Pt(II)) was purchased from Wuhan Yuancheng Gongchuang Technology Co., Ltd. Perfluorohexane (PFH) was purchased from Energy Chemical (Shanghai) Co., Ltd. 3-(Diethylamino)propylamine (DEAPA) was purchased from Aladdin Reagent (Shanghai) Co., Ltd. (2,3-Dioleoyloxy-propyl)-trimethylammonium (DOTAP) was from Ai Weituo (Shanghai) Pharmaceutical Technology Co., Ltd. 3-(4,5-Dimethyl-2-thiazolyl)-2,5-diphenyl tetrazolium bromide (MTT) was purchased from Yeli Biotechnology (Shanghai) Co., Ltd. Prussian Blue was purchased from Beyotime Biotechnology company. Survivin siRNA contained the antisense sequences of 5′-GCCTTTCCTTAAAGGCCATC-3′.

Synthesis of $PLGA_{12\,500}$–$mPEG_{2000}$

The preparation of $PLGA_{12\,500}$–$mPEG_{2000}$ was performed as previous.[16] In brief, 250.0 mg $PLGA_{12\,500}$ (2×10^{-5} mol) was dissolved in 7 mL DMSO, then 19.1 mg EDC·HCl (10×10^{-5} mol) and 11.5 mg NHS (10×10^{-5} mol) were added into the solution. After stirring solution for about 30 min at room temperature, 240.0 mg $mPEG_{2000}$–NH_2 (2×10^{-5} mol) was finally added, and the following was to be stirred for 4 h at room temperature. After using a dialysis bag with a molecular weight cutoff of 3500 to purify the product $PLGA_{12\,500}$–$mPEG_{2000}$ for one day, the dialyzed solution was freeze-dried to be stored.

Synthesis of DSPE–PEG_{1000}–Pt(IV)

The synthesis of DSPE–PEG_{1000}–Pt(IV) was described in the previous.[16] Briefly, 108.0 mg *cis*, *cis*, *trans*-[$PtCl_2(NH_3)_2$(-OH)(OOCCH$_2$CH$_2$COOH)] (0.25 mmol) was dissolved in 5 mL DMSO, and next 191.0 mg EDC·HCl (1 mmol) together with 115.0 mg NHS (1 mmol) was added into it; stir the solution at room temperature for 30 minutes and 435.0 mg DSPE–PEG_{1000}–NH_2 (0.25 mmol) was added into it and continued stirring for 72 h in the dark. Eventually, the solution was dialyzed with a dialysis bag whose molecular weight cutoff was 1000 for 24 h and then freeze-dried to get DSPE–PEG_{1000}–Pt(IV).

Modification of Fe_3O_4 nanoparticles

According to Xiao *et al.*,[18] the synthesis was as following. EDC·HCl (2.521 g, 13.200 mmol) and NHS (1.518 g, 13.200 mmol) were dissolved in 10 mL ultrapure water, next 10 mL Fe_3O_4 nanoparticles solution (containing 3.3 mmol COOH) was added, and then mix them together with 80 mL ultrapure water and start mechanical stirring at 250 rpm by digital mixer (IKA RW20). Finally, DEAPA (859 mg, 1.041 mL, 6.6 mmol) was added, and the reaction lasted for 4 hours. After the modification, the sample was subjected to ultrafiltrate to remove the

unreacted EDC, NHS, and DEAPA, thereby obtaining the zwitterionic modified superparamagnetic magnetic resonance contrast agent. And we used a Malvern Zetasizer Nano ZS (Malvern Instrument, Malvern, UK) to measure the zeta potential and size distribution of the modified Fe_3O_4 nanoparticles. Also, we explored the X-ray diffraction (XRD) and the magnetic character of Fe_3O_4 nanoparticles respectively by X-ray polycrystalline (powder) diffractometer (Bruker D8 advance) and Mettler Toledo DG115-SC.

Synthesis of PFH/siRNA/Fe_3O_4@Pt(IV) NPs-cRGD (NPs-cRGD)

10.2 mg $PLGA_{12\,500}$–$mPEG_{2000}$, 12.0 mg DSPE–PEG_{1000}–Pt(IV), 1.8 mg DOTAP and 6.0 mg $PLGA_{12\,500}$–PEG_{2000}–Mal were dissolved in 600 μL trichloromethane and next 30 μL PFH was added. After adding certain Fe_3O_4 nanoparticles and siRNA to make the final concentration of them in nanoparticles solution be 160 μg mL^{-1} and 400 nM respectively, ultrasound at 325 W was performed for one minute in an ice bath. After adding the above solution into 4 mL 1% PVA, the mixture was under the ultrasound at 550 W for 5 minutes in an ice bath and then under the mechanical stirring at room temperature for 4 hours. The free siRNA got cleared by ultrafiltrating at 5000 rpm for 1 hour,[19] and then two cycles of centrifugation by centrifuge (Eppendorf 5415) was used to purify the synthesized nanoparticles,[20] and lastly the nanoparticles were resuspended with adequate deionized water.

Characterization of NPs-cRGD

Zeta potential and size distribution of NPs-cRGD were measured by a Malvern Zetasizer Nano ZS. The morphology of NPs-cRGD located in ordinary carbon film were observed by transmission electron microscopy (TEM, Tecnal G2 Spirit Bio Twin, FEI company). Meanwhile, X-ray diffraction (XRD) of NPs-cRGD was performed by X-ray polycrystalline (powder) diffractometer and the magnetization was measured by a vibrating sample magnetometer (Lake Shore VSM 7307) in 298 K. The encapsulation rate of siRNA was calculated by the concentration of unencapsulated cy5-siRNA measured by fluorescence spectrometer (HITACHI F-2700). An inductively coupled plasma mass spectrometry (ICP-MS, Leeman Prodigy, USA) was used to measure the Pt(IV) drug loading capacity.

Storage stability of NPs-cRGD

The storage stability of NPs-cRGD was observed by measuring the size distribution and zeta potential of NPs-cRGD. After storing the nanoparticles in closed EP tubes at 4 °C for 1 to 14 days, the average size and zeta potential of them were regularly measured by dynamic light scattering every day.

Serum-induced aggregation assay

The aggregation was monitored by measuring turbidity.[20,21] In belief, free siRNA and NPs-cRGD containing the same concentration siRNA as free siRNA were mixed with equal PBS and 30% FBS (v/v), respectively. PBS and 30% FBS (v/v) were set as contrast and then all samples were incubated at 37 °C. The absorbance of samples at 500 nm were measured at 1 min, 5 min, 30 min, 1 h, 4 h, 8 h, 12 h, 24 h and 30 h, 2 d, 3 d, 4 d, 5 d, 6 d, 7 d by a ultraviolet spectrophotometer (Bio-Tek Synergy 2). A relative turbidity value of 1 indicated that the turbidity of the serum-incubated mixture was equal to the turbidity of the PBS-incubated sample.

Gel-retardation assay

In this experiment, we used the following to detect the stability of encapsulating situation and the protecting to siRNA. Briefly, 1% (w/v) agarose gel containing ethidium bromide loaded samples and next the samples were electrophoresed at 120 V for 20 min in 1× TAE buffer at pH 8.0 [10.0 mM Tris/HCl (pH 7.6), 1% (v/v) acetic acid, and 1.0 mM EDTA (pH 8.0)] and siRNA in 1% (w/v) agarose gel was visualized by a bioelectrophoresis image analysis system (FR-980A). In order to explore the protecting of NPs-cRGD to siRNA, we set four groups including free siRNA, free siRNA with RNase, NPs-cRGD and NPs-cRGD with RNase. 20 μL samples were removed at 0 min, 30 min, 2 h, 4 h, 8 h, 1 d, 3 d, 5 d to observe the existence and location of siRNA.

In vitro MRI of NPs-cRGD

In order to observe the negative MRI of NPs-cRGD, NPs-cRGD with several different iron concentrations which were 2.5, 5, 10, 20, 40, 80, 160, 320 μg mL^{-1} were prepared in 1.5 mL EP tubes to measure the T_2 value by nuclear magnetic resonance imaging analyzer (NMI20-015V-I) and T_2-weighted imaging by nuclear magnetic resonance imaging analyzer (MesoMT23-060H-I).

In vitro US imaging of NPs-cRGD

The relation between the concentration of Fe_3O_4 nanoparticles and the ultrasound imaging of NPs-cRGD was measured in plastic gloves by a VisualSonics 2100 imaging system with a MS-201 transducer (VisualSonics Inc., Canada). Saline was used as blank control. Next, we selected the optional concentration of Fe_3O_4 nanoparticles and then changed the concentration of NPs-cRGD to observe the US imaging. Besides, we explored the duration time of ultrasound imaging of NPs-cRGD.

Cell culture

The SKOV3 human ovarian tumor cell line was provided by the Cell Resource Center, Shanghai Institutes for Biological Sciences (SIBS, Shanghai, China). The L929 cell was purchased from Shanghai Academy of Sciences Cell Bank. SKOV3 cell and L929 cell was cultured in DMEM containing 10% FBS (v/v), 1% penicillin/streptomycin (v/v) and incubated at 37 °C in a 5% CO_2 environment.

Safety assessment *in vitro*

After seeding 1×10^5 SKOV3 cells or L929 cells into a well of 96-well plates and incubating with complete DMEM medium (37 °C, 5% CO_2) for 24 h, the medium was removed. 100 μL nanoparticles DMEM medium mixture without connecting Pt(IV) and encapsulating siRNA whose concentrations were

respectively 0, 5, 10, 25, 50, 100, 250, 500, 1000 μg mL^{-1} were added into each well, and each concentration had six parallel wells and then the cells were incubated for 24 h, 48 h and 72 h. Next the cell viability was measured by MTT method.

Cytotoxicity assay

The antitumor efficiency of different nanoparticles were measured by MTT assay. In brief, after seeding 1×10^5 SKOV3 cells or L929 cells into a well of 96-well plates and incubating with complete DMEM medium (37 °C, 5% CO_2) for 24 h, the medium was removed. 100 μL different concentrations NPs-cRGD in which the concentrations of Pt(IV) were 0.3, 3, 6, 12, 24, 48, 96, 192 μM were added into every well and each concentration had six parallel wells and then the cells were incubated for 24 h, 48 h and 72 h. Then the cell viability was measured by MTT method. Also, at the same time, we explored the killing effects of free cisplatin, PFH/siRNA/Fe_3O_4@Pt(IV) NPs (NPs) and NPs-cRGD together with ultrasound (NPs-cRGD + US). The assay was repeated for three times.

Prussian blue staining

1×10^5 SKOV3 cells were seeded into a well of 96-well plates and incubated with complete DMEM medium (37 °C, 5% CO_2) for 24 h, then the medium was removed. 100 μL free Fe_3O_4 nanoparticles and different nanoparticles containing Fe_3O_4 nanoparticles which were respectively NPs, NPs-cRGD and NPs-cRGD + US were added. The concentrations of iron in nanoparticles were 80 and 640 μg mL^{-1} and each concentration had three parallel wells. After incubated for 24 h, the cells were washed with PBS for three times, fixed with 4% paraformaldehyde for 20 min, incubated with Pearls reagent (4% potassium ferrocyanide and 12% HCl, 50 : 50 vol/vol) for 60 min at room temperature, and then incubated with nuclear fast red for 3 minutes, and washed with PBS for three times. The samples were observed under a light microscope (Olympus IX51) to know the quality of intracellular iron. Each assay was repeated for three times.

Statistical analysis

All results were expressed as the mean value ± standard deviation (SD) of three independent measurements. Analysis of variance (ANOVA) was performed when more than two groups were compared, and when the result was significant ($P < 0.05$), multiple comparisons were performed using Tukey's post hoc test. All statistical analyses were performed with GraphPad Prism (7.0). $^*P < 0.05$, $^{**}P < 0.01$, $^{***}P < 0.005$.

Conclusions

In this study, we successfully constructed the nanoparticles (PFH/siRNA/Fe_3O_4@Pt(IV) NPs-cRGD) with the capacity of dual-mode US/MRI imaging and improving treatment to ovarian cancer. NPs-cRGD possessed good storage stability and resisted the serum-induced aggregation and nuclease degradation. Both the MRI and US imaging experiments demonstrated that NPs-cRGD exhibited an excellent dual-mode US/MRI imaging. Besides, the *in vitro* experiments indicated that NPs-cRGD with US exhibited brilliant antitumor therapeutic efficiency. Thus, the dual-mode nanoparticles in this work may provide precious insight into the development of various multi-mode nanoplatforms for precise theranostics against various cancer.

However, there is still lots of work to be further studied, such as the phase shifting behavior of PFH, the impact of iron on the conversion efficiency, the apoptosis of cells treated with nanoparticles, the cellular metabolism mechanism of Pt(IV) and siRNA, the expression of some oncogenes and tumor suppressor genes, the expression of proteins related to the cell death pathway, the imaging and therapy efficiency *in vivo* and the side effect. We intend to do the further research in our future work to explain the improvement of treatment and relative imaging details.

Conflicts of interest

There are no conflicts of interest to declare.

Acknowledgements

The authors acknowledge financial support from NSFC/China (No. 81572999, No. 81771839, No. 81773272 and No. 81874479).

Notes and references

1 R. Siegel, K. Miller and A. Jemal, *Ca-Cancer J. Clin.*, 2019, **69**, 7–34.
2 A. Cortez, P. Tudrej, K. Kujawa and K. Lisowska, *Cancer Chemother. Pharmacol.*, 2018, **81**, 17–38.
3 R. Ozolvs and R. Young, *Curr. Probl. Cancer*, 1987, 8.
4 J. Hainsworth, L. Burnett, H. Jones III, W. Grosh, D. Johnson and F. Anthony Greco, *J. Clin. Oncol.*, 1990, **8**, 502–508.
5 M. Apps, E. Choi and N. Wheate, *Endocr.-Relat. Cancer*, 2015, **22**, 219–233.
6 M. Maurie, *Trends Pharmacol. Sci.*, 2008, **29**, 515–519.
7 C. Huang, Y. Sun, M. Shen, X. Zhang, P. Gao and Y. Duan, *ACS Appl. Mater. Interfaces*, 2016, **8**, 1360–1370.
8 S. Yoong, B. Wong, Q. Zhou, C. Chin, J. Li, T. Venkatesan, H. Ho, V. Yu, W. Ang and G. Pastorin, *Biomaterials*, 2014, **35**, 748–759.
9 H. Xiao, H. Song, Y. Zhang, R. Qi, R. Wang, Z. Xie, Y. Huang, Y. Li, Y. Wu and X. Jing, *Biomaterials*, 2012, **33**, 8657–8669.
10 G. Nora and S. Lippard, *Adv. Drug Delivery Rev.*, 2012, **64**, 993–1004.
11 J. Reyes-González, G. Armaiz-Peña, L. Mangala, F. Valiyeva, C. Ivan, S. Pradeep, I. Echevarría-Vargas, A. Rivera-Reyes, A. Sood and P. Vivas-Mejía, *Mol. Cancer Ther.*, 2015, **14**, 2260–2269.
12 S. Kala, A. Mak, X. Liu, P. Posocco, S. Pricl, L. Peng and A. Wong, *J. Med. Chem.*, 2014, **57**, 2634–2642.
13 K. Togashi, M. Okada, M. Yamamoto, S. Suzuki, T. Sanomachi, S. Seino, H. Yamashita and C. Kitanaka, *Anticancer Res.*, 2018, **38**, 4535–4542.
14 J. Dynek and D. Vucic, *Cancer Lett.*, 2013, **332**, 206–214.

15 X. Li, J. Pang, Y. Li, F. A. Ahmed, R. He, J. Ma, F. Ma and G. Chen, *Pathol., Res. Pract.*, 2018, **214**, 385–401.
16 H. Huang, Y. Dong, Y. Zhang, D. Ru, Z. Wu, J. Zhang, M. Shen, Y. Duan and Y. Sun, *Theranostics*, 2019, **9**, 1047–1065.
17 Y. Zhou, Z. Wang, Y. Chen, H. Shen, Z. Luo, A. Li, Q. Wang, H. Ran, P. Li, W. Song, Z. Yang, H. Chen, Z. Wang, G. Lu and Y. Zheng, *Adv. Mater.*, 2013, **25**, 4123–4130.
18 W. Xiao, J. Lin, M. Li, Y. Ma, Y. Chen, C. Zhang, D. Li and H. Gu, *Contrast Media Mol. Imaging*, 2012, **7**, 320–327.
19 Y. Teng, M. Bai, Y. Sun, Q. Wang, F. Li, J. Xing, L. Du, T. Gong and Y. Duan, *Int. J. Nanomed.*, 2015, **10**, 5447–5457.
20 Y. Zhang and T. Anchordoquy, *Biochim. Biophys. Acta*, 2004, **1663**, 143–157.
21 J. Chen, P. Gao, S. Yuan, R. Li, A. Ni, L. Chu, L. Ding, Y. Sun, X. Liu and Y. Duan, *ACS Nano*, 2016, **10**, 11548–11560.
22 J. Zhang, B. Li, W. Yang and J. Liu, *Ind. Eng. Chem. Res.*, 2014, **53**, 10629–10636.
23 J. Lee, D. Carugo, C. Crake, J. Owen, M. Victor, A. Seth, C. Coussios and E. Stride, *Adv. Mater.*, 2015, **27**, 5484–5492.
24 P. Dubey, M. Vivek, J. Sanyog, M. Suunil and S. Vyas, *J. Drug Targeting*, 2004, **12**, 257–264.
25 Z. Li, H. Huang, L. Huang, L. Du, Y. Sun and Y. Duan, *Int. J. Mol. Sci.*, 2017, **18**, 815–830.
26 Z. Ge, Q. Chen, K. Osada, X. Liu, T. Tockary, S. Uchida, A. Dirisala, T. Ishii, T. Nomoto, K. Toh, Y. Matsumoto, M. Oba, M. Kano, K. Itaka and K. Kataoka, *Biomaterials*, 2014, **35**, 3416–3426.